

AN EXPERIMENTAL STUDY OF AERODYNAMICALLY
VARIABLE THROAT AREA (AVT) NOZZLES

By

WILLIAM N. JACKOMIS

Bachelor of Science

University of Notre Dame

Notre Dame, Indiana

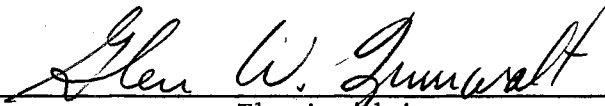
1954

Submitted to the faculty of the Graduate School of
the Oklahoma State University
in partial fulfillment of the requirements
for the degree of
MASTER OF SCIENCE
August, 1962

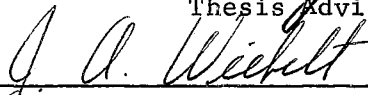
NOV 8 1962

AN EXPERIMENTAL STUDY OF AERODYNAMICALLY
VARIABLE THROAT AREA (AVT) NOZZLES


Thesis Approved:



Thesis Adviser



J. A. Wickelt



Dean of the Graduate School

504518

ACKNOWLEDGEMENT

The author wishes to take this opportunity to express his sincere appreciation and gratitude to his academic adviser, Dr. Glen W. Zumwalt, a truly talented and outstanding educator, for his genuine interest and suggestions. His guidance, encouragement, and instruction have proven invaluable in the accomplishment of this thesis.

Acknowledgement is also extended to the Mechanical Engineering Faculty and to those in the Mechanical Engineering and Research Laboratories whose cooperation and assistance during all phases of this research were of extreme value.

Appreciation is also extended to the United States Air Force, whose educational programs have made this advanced study possible.

In accord with this opportunity, the author wishes to express appreciation to his mother, whose encouragement has supplied faith and hope during this endeavor.

The author would be remiss if he failed to mention the sacrifices made during the preparation of this thesis by his wife, Bobbie, and his two daughters, Patti and Terri, to whom this paper is dedicated.

TABLE OF CONTENTS

Chapter	Page
I. INTRODUCTION.	1
II. ANALYSIS OF THRUST CONTROL BY THROAT AREA VARIATION.	3
III. COLD AIR TESTS OF AERODYNAMICALLY VARIABLE THROAT AREA (AVT) NOZZLES	10
IV. TEST RESULTS.	16
V. EXAMPLE OF APPLICATION TO A SPECIFIC ROCKET	18
VI. CONCLUSIONS AND RECOMMENDATIONS	20
SELECTED BIBLIOGRAPHY.	22
APPENDIX	23

LIST OF FIGURES

Figure	Page
1. The AVT Nozzle on a Solid Propellant Rocket.	24
2. Equilibrium Pressure Conditions for a Solid Propellant Rocket.	25
3. The AVT Nozzle for Air Flow Tests.	26
4. Detailed View of Conical Expansion Section of AVT Nozzle.	27
5. Detailed View of Inlet Section of AVT Nozzle	28
6. Schematic of Test Set-up	29
7. Primary Flow Change for Secondary Flow Rates (Air Flow Tests)	30
8. Primary Flow Change for Secondary Flow Rates (Air Flow Tests, $\alpha = 0$ Degrees).	31
9. Primary Flow Change for Secondary Flow Rates (Air Flow Tests, $\alpha = -15$ Degrees).	32
10. Primary Flow Change for Secondary Flow Rates (Air Flow Tests, $\alpha = +15$ Degrees).	33
11. Comparison of Primary Flow Changes for Secondary Flow Rates (Air Flow Tests, $\alpha = 0, -15, +15$ Degrees)	34
12. Effect of Secondary Supply Pressure on Primary Flow Change (Air Flow Tests, $\alpha = 0$ Degrees).	35
13. Calculated Thrust Ratio for the Example Rocket at Sea Level	36
14. Calculated Thrust Ratio for the Example Rocket in a Vacuum.	37
15. Calculated Chamber Pressure Ratio for the Example Rocket	38
16. AVT Nozzles Used in Tests.	39

Figure	Page
17. Thrust Stand Apparatus	40
18. Thrust Stand Apparatus with Ejector in Position.	41
19. Thrust Stand Control Panel Arrangement Used in Tests.	42

LIST OF SYMBOLS

A_e	flow area at nozzle exit
A_t	flow area at nozzle throat
b	constant in Equation (1)
C_c	contraction coefficient
C_D	nozzle discharge coefficient
C_F	thrust coefficient
C_v	velocity coefficient (ratio of ideal to actual pressure drop)
c^*	characteristic velocity
F	thrust
g	gravitational constant
$H_{f,2}$	sum of energy losses due to flow constriction and pipe wall friction
k	ratio of specific heats
\dot{M}_e	mass rate of gas exhausting from nozzle
\dot{M}_g	mass rate of gas produced by combustion
\dot{M}_s	mass rate of gas stored in combustion chamber
\dot{M}_1	mass flow rate of primary gas with secondary flow
\dot{M}_2	mass flow rate of secondary flow
\bar{m}	molecular weight
n	pressure exponent in Equation (1)
p_a	static pressure of atmosphere
p_e	static pressure at nozzle exit
P_c	total pressure in the combustion chamber

p^*	stream pressure at throat
R	gas constant
r	linear burning rate
S	propellant burning surface area
T_c	total temperature in combustion chamber
t^*	stream temperature at the throat
V_e	velocity at nozzle exit
V_j	equivalent jet velocity
V^*	velocity at nozzle throat
α	secondary injection flow angle relative to primary flow
ρ_g	density of gas
ρ_p	density of propellant
μ	dynamic viscosity

Subscripts

$1,2$	refers to conditions upstream and downstream, respectively, from the metering device
-------	-----------------------------------------------------------------------------------------

CHAPTER I

INTRODUCTION

The complexities which are inherent in liquid propellant powerplants have motivated scientists to experiment with many types of fuels. Solid fuels, long ignored, are now moving into the forefront of missile design because of their tremendous advantage in simplicity, storeability, and ease of handling. Because of these apparent advantages, the United States has produced solid-propellant rockets such as the Navy's Polaris and the Air Force's Minuteman.

Where adherence to specified trajectories and velocities are necessary, such as in ballistic missiles and space vehicles, the advantages of thrust magnitude control are important. It is conceivable that the ultimate choice between a solid or a liquid propellant may depend upon the guidance system required, rather than on the merits of the powerplant. This could possibly be influenced by the development of thrust control for solid propellant rockets.

In the competition with liquid-fueled rockets, the solid propellant rocket has suffered from the disadvantage of lack of thrust control once ignition has occurred. The thrust control problem divides itself into three types:

- (a) thrust predictability
- (b) thrust directional control
- (c) thrust magnitude control

For each of these three types of control, solid propellant rockets present difficulties beyond those of liquid-fueled rockets; and these have sometimes overshadowed the solid's inherent advantages. It is the third of these problems which still seeks a successful approach, and with which this paper shall deal.

Although no positive system for controlling thrust variation in solid-propellant rockets can be found in the literature, several systems and theories have been empirically exploited. In addition to suggestions calling for mechanical means of covering and exposing the propellant burning surface, burning rate control by acoustical energy variation has been studied and tested by Summerfield (1)¹. Since the most useful variables for controlling thrust variations are 1) burning surface, 2) linear burning rate, and 3) nozzle throat area, the most attractive means for most investigators is the nozzle throat area variation. Berman and Crimp (2) suggested that the plug nozzle could achieve thrust control by axial movement of the plug. Gates and Pinto (3) proposed a mechanical iris-type variable throat; and the expansion-deflection nozzle of Rao (4) has been suggested as a possible variable throat area nozzle by axial movement of the deflecting centerbody.

These and many other similar proposed plans all share one limitation: the difficulty of performing mechanical movement reliably at the temperatures found in rocket nozzle throats. The method proposed in this thesis utilizes a non-mechanical means of achieving nozzle area change and is believed to possess the potential of becoming an extremely powerful tool in the accomplishment of specified space trajectories and orbital paths where solid propellant rockets are used.

¹() Refers to Selected Bibliography.

CHAPTER II

ANALYSIS OF THRUST CONTROL BY THROAT AREA VARIATION

If a secondary flow of gas is injected radially inward at or near the throat of a thrust nozzle, the primary flow streamlines are displaced inwardly, effectively decreasing the throat area. The injection can be accomplished through a thin slit or a series of holes around the throat. This nozzle is termed an aerodynamically-variable throat (AVT) nozzle and is shown in Figure 1.

To consider an approximate analysis, we shall make use of the fact that the linear burning rate, r , of a solid propellant rocket is a characteristic property of the propellant. It is primarily a function of the chamber static pressure, P_c , and the temperature, T_p , of the propellant grain. It may be written as:

$$r = f(P_c, T_p)$$

For a fixed value of propellant temperature, the burning rate equation is expressed by

$$r = b(P_c)^n \tag{1}$$

where b and n are constants whose magnitudes depend on the chemical composition of the solid propellant. For conventional solid propellants, the value of n ranges from 0.2 to 0.8, the larger values being associated with the faster burning propellants. Stable burning will occur only for n values less than unity. Further, the exhaust gases shall be treated as perfect gases, with constant chemical composition, gas

constant, and specific heat ratios while in the nozzle. The temperature of the combustion gas in the chamber, T_c , shall be considered independent of chamber pressure, P_c , for moderate changes in pressure.

Since the burning rate is a function of the chamber pressure, P_c , and is directly proportional to the thrust level, a system designed to control the chamber pressure would also control the thrust. The equilibrium chamber pressure occurs when the mass rate of gas produced by combustion, M_g , equals the sum of the mass rates of gases exhausted, M_e , plus the mass rate of gases stored, M_s , or

$$M_g = M_e + M_s. \quad (2)$$

The mass rate of flow exhausted, M_e , through the nozzle is proportional to the chamber pressure, P_c , times the throat area, A_t , for a constant burning temperature. This may be derived as follows:

$$M_e = [\rho^* V^* A_t] C_d = \frac{p^*}{R t^*} \sqrt{2 g J c_p (T_c - t^*)} A_t C_d$$

where
$$p^* = P_c \left[\frac{2}{k+1} \right]^{\frac{k}{k+1}},$$

$$t^* = T_c \left[\frac{2}{k+1} \right],$$

$$\rho^* = \rho_c \left[\frac{p^*}{P_c} \right]^{\frac{1}{k}} = \rho_c \left[\frac{2}{k+1} \right]^{\frac{1}{k+1}},$$

$$J c_p = \left[\frac{k}{k-1} \right] R.$$

$$\text{Hence, } M_e = \frac{p^* A_t C_d}{R T_c} \left[\frac{T_c}{t^*} \right] \sqrt{2 g R \frac{k}{k-1} T_c \left[1 - \frac{t^*}{T_c} \right]}.$$

Rearranging terms yields

$$M_e = \frac{p^* A_t C_d}{\sqrt{RT_c}} \left[\frac{k+1}{2} \right] \sqrt{2g \left[\frac{k}{k-1} \right] \left[1 - \frac{2}{k+1} \right]}$$

$$= \frac{p^* A_t C_d}{\sqrt{RT_c}} \left[\frac{k+1}{2} \right] \sqrt{2g \frac{k}{k+1}}$$

$$\text{Therefore, } M_e = C_d P_c A_t \sqrt{\frac{gk}{RT_c}} \left[\frac{2}{k+1} \right]^{\frac{k+1}{2(k-1)}} \quad (3)$$

Alternately, the dependence of M_e on P_c and A_t can be shown from considering the effectiveness with which combustion produces high-temperature, high-pressure gases. The measure of this is the characteristic velocity, c^* , (defined as $c^* = V_j/C_F$) which is a function of P_c , A_t , and M_e :

$$c^* = \frac{V_j}{C_F} = \frac{g F/M_e}{F/P_c A_t} = \frac{P_c A_t g}{M_e} \quad (4)$$

The characteristic velocity, c^* , can also be shown to be a function of the related chamber temperature, T_c , the ratio of specific heats, k , and the molecular weight, \bar{m} , that is: $c^* = f(T_c, k, \bar{m})$.

We have shown that $c^* = \frac{P_c A_t g}{M_e}$ and $M_e = \rho^* V^* A_t$.

Now substituting for M_e , we have

$$c^* = \frac{P_c A_t g}{\rho^* V^* A_t} = \frac{P_c}{\rho^*} \frac{g}{V^*} = \frac{P_c}{P^*} \frac{g R t^*}{\sqrt{k g R t^*}}$$

where $V^* = \sqrt{kgRt^*}$,

$$t^* = T_c \left[\frac{2}{k+1} \right] ,$$

$$R = \frac{1545}{\bar{m}} .$$

therefore, $c^* = \sqrt{\frac{kg}{k}} \left[\frac{2}{k+1} \right]^{-\frac{k}{k-1}} \sqrt{Rt^*}$

$$= \sqrt{\frac{kg}{k}} \left[\frac{2}{k+1} \right]^{\frac{-(k+1)}{2(k-1)}} \sqrt{\frac{1545}{\bar{m}}} \sqrt{T_c} .$$

Thus, c^* is constant for the assumed constant T_c .

Equation (3) may now be written as

$$M_e = \frac{P_c A_t g}{c^*}$$

or simply that $M_e \sim P_c A_t$. (5)

The mass rate of gases produced by combustion, M_g , is proportional to $(P_c)^n$ and may be expressed as follows:

$$M_g = r S \rho_p . \quad (6)$$

Substituting equation (1) into equation (6) yields the rate of gas produced as

$$M_g = b(P_c)^n S \rho_p , \text{ or simplifying,} \quad (7)$$

we conclude that

$$M_g \sim (P_c)^n . \quad (8)$$

The mass rate of gases stored, M_s , may be expressed as

$$M_s = r S \rho_g . \quad (9)$$

If the gas density is small compared to that of the propellant, we may neglect the mass storage rate as compared to the other two terms.

Substituting the related expressions of equation (3) and (7) for each value in equation (1) then yields

$$b(P_c)^n S \rho_p = C_d P_c A_t \sqrt{\frac{gk}{RT_c}} \left[\frac{2}{k+1} \right]^{\frac{k+1}{2(k-1)}} \quad (10)$$

Solving for P_c gives

$$P_c = \left[\frac{1}{b} \frac{A_t}{\rho_p S} \frac{C_d}{\sqrt{T_c}} \sqrt{\left[\frac{kg}{R} \right] \left[\frac{2}{k+1} \right]^{\frac{k+1}{k-1}}} \right]^{\frac{1}{n-1}} \quad (11)$$

Thus, under the simplifications made,

$$P_c \sim (A_t)^{\frac{1}{n-1}}$$

and $M_e \sim P_c A_t$

or $M_e \sim (A_t)^{\frac{n}{n-1}} \quad (12)$

Thus, it is shown that the chamber pressure, P_c , is related to the throat area, A_t , of the nozzle by the exponential value $\frac{1}{n-1}$. As indicated by equation (10), stable operating conditions occur when the mass rates are equal. Figure 2 shows the plot of mass rate versus chamber pressure for an n value less than unity. It can readily be seen that a reduction in nozzle throat area, A_t , will increase both the mass rate and the chamber pressure, P_c , thereby increasing thrust. If a high exponent fuel is used, for example, $n = 0.9$, this effect becomes very pronounced and a great thrust increase should be realized. It should be noted, however, that the combustion process for a solid-propellant with $n < 1$ is inherently self-regulating with respect to small deviations in the burning pressure.

The nozzle thrust is given by

$$F = M_e V_e + (p_e - p_a) A_e \quad (13)$$

or
$$F = C_F P_c A_t \quad (14)$$

In equation (13), p_a and A_e are unaffected by throat area change. For constant chamber temperature, V_e is only slightly affected by a throat area change induced by secondary air injection, since the secondary air occupies a portion of the flow area at the exit as well, tending to keep effective flow area ratio, A_e/A_t , constant. This is substantiated by noting equation (14). It is known that C_F is not sensitive to nozzle area ratio changes for reasonably high values of A_e/A_t and p_e/p_a . Therefore:

$$F = M_e V_e + \frac{p_e}{P_c} P_c A_e - p_a A_e, \text{ or we may say that}$$

$$F = f \left[(A_t)^{\frac{n}{n-1}} V_e + \frac{p_e}{P_c} A_e (A_t)^{\frac{n}{n-1}} - p_a A_e \right] \quad (15)$$

where $\frac{p_e}{P_c}$ is a function of nozzle area ratio and fluid properties.

If we give the subscript o to the equilibrium burning conditions associated with the original throat area, A_{t_o} , and let the terms without o subscripts refer to values associated with equilibrium burning for the changed area, A_t , then

$$\frac{P_c}{P_{c_o}} = \left[\frac{A_t}{A_{t_o}} \right]^{\frac{1}{n-1}} \quad (16)$$

$$\frac{M_e}{M_{e_o}} = \left[\frac{A_t}{A_{t_o}} \right]^{\frac{n}{n-1}} \quad (17)$$

$$\frac{F}{F_o} = \frac{M_e V_e \left[\frac{A_t}{A_{t_o}} \right]^{\frac{n}{n-1}} + \frac{p_e}{P_c} A_e P_{c_o} \left[\frac{A_t}{A_{t_o}} \right]^{\frac{1}{n-1}} - p_a A_e}{M_{e_o} V_e + \frac{p_e}{P_c} A_e P_{c_o} - p_a A_e} \quad (18)$$

The effect of throat area reduction is illustrated in Figure 2. The equilibrium (stable) conditions are represented by the intersections of the curves. The smaller throat area results in the larger chamber pressure and mass flow rate, and therefore, in larger thrust. This possibility was noted by Rodriguez (5) in his paper on side injection for thrust direction control.

CHAPTER III

COLD AIR TESTS OF AERODYNAMICALLY VARIABLE

THROAT AREA (AVT) NOZZLES

Tests of the nozzles shown in Figures 3, 4, 5, and 16, were run on the nozzle thrust stand of the Gas Dynamics Laboratory at Oklahoma State University. During the course of this experimental study, three nozzle designs were considered. These designs were selected so as to determine the throat area effects of radial secondary flow injection in several different directions relative to the main flow through the nozzle. Secondary injection angles, termed alpha (α), were selected for 0, +15, and -15 degrees of flow relative to the primary flow throat plane through the nozzles. The throat diameter of each of these nozzles was 0.55 inches and nozzle exit area ratios were selected to be 12 to 1. All the nozzles were constructed and machined from 2 1/4 inch solid brass stock.

The AVT nozzles used in these tests were designed and constructed in two separate sections, as shown in Figure 3, in order to control the mass rate of flow of the secondary flow stream. The nozzles were separated at the throat perpendicular to the nozzle axis, a torus cavity and an arc inlet corresponding to the secondary flow angle desired were machined, and a secondary air supply line attached. The nozzle throats were preceded by elliptical inlet sections and followed by conical expansion sections. Detailed drawings of the components of these nozzles

are shown in Figures 4 and 5. The expansion and inlet sections of the nozzles were held rigidly in place by using four screws countersunk into the rim at the base of the inlet section of the nozzles. Alignment of the two sections of each nozzle was accomplished by using two alignment pins so that smooth internal passages were achieved for the tests. This is clearly shown in Figures 4 and 5. Room temperature primary air was supplied and sufficient pressure ratio applied to insure shock-free flow to the nozzle exits.

Since the area ratio of these nozzles was 12 to 1, it was necessary to use an ejector system to locally lower the exhaust back pressure below atmospheric. This ejector system consists of an ejector tube mounted to encompass the rocket nozzle exhaust jet. This is shown in Figures 17 and 18. Figure 17 shows the ejector assembly on the sliding mounts, while Figure 18 shows the ejector assembly encompassing the nozzle in its operating condition. As the flow exits from the nozzle, it diverges slightly; and the jet boundary attaches to the ejector wall deflecting in a shock wave. As air is entrained in the free jet, a diffuser action raises the pressure to atmospheric and the shock waves are pulled inside the ejector tube. As additional air is thus entrained, a higher vacuum is pulled until a stable pressure ratio is reached.

Thrust was not measured because of difficulty in obtaining shock-free flow in the nozzles for all runs. Also, extremely small thrust changes are experienced from throat injection in simple air flow systems, since no change in gas production rate occurs as in a solid propellant rocket. Thus, the test runs were solely for the purpose of evaluating effective throat area change.

The torus-shaped cavities in the conical expansion section of the nozzles served to supply high velocity secondary air to the nozzle throats.

The chambers were supplied by a separate air source in the laboratory and allowed the pressure of the secondary air to reach equilibrium in the torus before being discharged in a 360° radial pattern into the main nozzle throat. The insertion of shims of thicknesses of 0.003, 0.007, 0.010, and 0.013 inches between the two sections of the nozzles provided variation in the slit width for secondary flow. Primary and secondary mass flow rates were measured for various slit widths and secondary-to-primary total pressure ratios. A schematic drawing of the test equipment is shown as Figure 6.

In order to determine the mass flow of air entering the main stream of the nozzle, a flow metering nozzle was employed. This metering nozzle was designed according to ASME Flow Measurement Code, 1956, and is a basic component of the Thrust Stand Facility in the Gas Dynamics Laboratory.

The basic principle involved in determining the mass-rate of flow is to introduce a constriction into the pipe to produce a change in pressure. The approximate relationship between the pressure change and the rate of flow, assuming one-dimensional flow, is found by application of the energy and continuity equations across the metering nozzle. If the relative pressure change is small, density changes can be neglected. The energy equation may then be written as

$$\frac{P_2 - P_1}{\rho_1 g} + \frac{V_2^2 - V_1^2}{2g} + H_{f1,2} = 0 \quad (19)$$

where section 1 is upstream of the constriction and 2 is in the constriction itself. The continuity equation may be considered as

$$A_1 V_1 = A_2 V_2. \quad (20)$$

Combining equations (19) and (20) and solving for V_2 yields

$$V_2 = \frac{1}{\sqrt{1 - \left[\frac{A_2}{A_1}\right]^2}} \sqrt{\frac{2(P_1 - P_2)}{\rho} - 2gH_{1,2}} \quad (21)$$

For a given rate of flow, the pressure drop will be decreased by $H_{1,2}$. Using the velocity coefficient, C_v , equation (21) may be written as

$$V_2 = \frac{C_v}{\sqrt{1 - \left[\frac{A_2}{A_1}\right]^2}} \sqrt{\frac{2(P_1 - P_2)}{\rho}} \quad (22)$$

Since $m = A_2 V_2$, we may substitute for V_2 and equation (22) then becomes

$$m = \frac{A_2 C_v}{\sqrt{1 - \left[\frac{A_2}{A_1}\right]^2}} \sqrt{\frac{2(P_1 - P_2)}{\rho}} \quad (23)$$

A pressure tap located in the pipe wall downstream of the metering nozzle may not yield the pressure at the nozzle throat due to the eddying that occurs in the dead-air region surrounding the jet. Also, because of the curvature of flow as the stream contracts through the nozzle, the pressure at the wall upstream from the nozzle varies slightly with the distance from the nozzle. By absorbing the factor $1/\sqrt{1 - \left[\frac{A_2}{A_1}\right]^2}$ into a new "discharge coefficient," C , we may write equation (23) as

$$m = A_2 C \sqrt{\frac{2}{\rho}(\Delta p)} \quad (24)$$

Since the pressure drop, Δp , depends upon m , ρ , A_1 , A_2 , and μ , we may conclude that

$$C = f \left[\frac{\rho V_1 D_1}{\mu}, \frac{A_2}{A_1} \right] \quad (25)$$

This implies that the discharge coefficient is a function of Reynold's Number and the area ratio, which may be calculated. From the graphs of the ASME Test Code, the discharge coefficient may be determined and hence, from equation (24), obtain the actual mass flow. (6). The accuracy of the calculations obtained in this manner were checked by comparison with mass flow rates calculated through the thrust nozzles.

The flow metering nozzle used in the thrust stand set-up for this experiment was installed in schedule 40, three-inch pipe between two flanges held rigidly in place by six 5/8-inch bolts. The area of the in-line nozzle was 0.5565 square inches. Pressure tap connections were installed both upstream and downstream of the nozzle and attached to a Mercury manometer to read differential pressure directly.

A sharp-edged plate orifice was used in this analysis to determine the mass flow of secondary air injected into the nozzle throats. The plate orifice was machined from stainless steel stock and fitted, using two O-ring seals, between two flanges attached to two lengths of 3/4-inch stainless steel pipe. Stainless steel was selected because of its durability and resistance to erosion.

The orifice was chosen to have a 1/4-inch inside diameter with knife-edge angles of 20 degrees. Two pressure taps were installed; one placed two pipe diameters upstream and the other placed 1/16-inch downstream from the orifice. Calibrated pressure gauges were attached to each of the pressure taps in order to determine the pressure differential needed for the mass flow calculations. This entire orifice arrangement was mounted in the line leading from the secondary air source to the nozzle throat. This is shown in the schematic drawing of Figure 6. Calibration was performed by use of a regulated constant flow gas meter connected in series with the orifice meter.

The principles involved in the determination of mass flow using the plate orifice are very similar to those developed for the metering nozzle. The only difference is that the discharge coefficient, C , for the orifice includes the correction factor for the contraction of the jet flow. The flow contracts after leaving the orifice and reaches the "vena contracta." For application to the orifice, equation (24) may be used and the mass rate of flow of secondary air determined.

CHAPTER IV

TEST RESULTS

Since the AVT nozzles used in these tests were the simple ellipse-cone type, they were sharp-cornered at the throat. The usual curvature of the sonic line near the wall would indicate that the injection slits may be in a slightly supersonic region. Secondary chamber pressure with zero secondary flow showed this to be true, with a pressure of about $0.35P_1$, corresponding to $M = 1.32$. Such a condition is not ideal for the AVT nozzles, which should perform better with injection slightly upstream of the sonic line. Nevertheless, the data of Figure 7 were obtained for various slit width thicknesses using the nozzle with secondary injection normal to the main stream. Here, the M_0 is the primary mass flow rate with zero secondary flow, M_1 is the primary flow rate with secondary flow rate of M_2 . Thus, Figure 7 shows per cent change in primary flow vs per cent secondary injected flow. It is seen that slit width is not a significant factor. For this nozzle, the amplification of mass flow effect is about 1.8. Figure 8 shows data points obtained at a later date using the same nozzle and serves to verify the curve of Figure 7.

Figure 9 illustrates the data obtained using a secondary injection angle of 15 degrees upstream of the throat plane. For this nozzle, amplification of mass flow effect is about 1.5. Figure 10 illustrates the data obtained using a secondary injection angle of 15 degrees down-

stream of the throat plane. For this nozzle, amplification of mass flow effect is about 0.67. Note also the shift of the zero-effectiveness on the abscissa for normal and downstream injection.

Figure 11 illustrates the comparison of primary flow changes for secondary flow rates for all three variations in nozzle design. As can readily be seen, the nozzle having a 15 degree downstream secondary injection is the least desirable of the three since amplification is very low.

Figure 12 illustrates the required secondary supply pressure for a given mass flow change for the largest and smallest slit widths. Large mass flow changes can result from secondary supply pressures no greater than the primary. Thus, the combustion chamber itself could supply the secondary gas, or it could supply gas for displacement pumping of another fluid.

In the cold air tests, primary supply temperature and pressure are the same for M_0 and M_1 . Therefore, $\frac{M_0 - M_1}{M_0}$ is an exact measure of the effective throat area change, $\frac{A_{t0} - A_t}{A_{t0}}$.

Rodriquez (5) describes his attempt to produce side forces by injecting secondary air just upstream of the throat through six holes extending over only 75% of arc. Virtually no side force resulted due to the opposite effects on pressure upstream and downstream of the throat. Specific thrust, based on total mass flow, primary plus secondary, was not measurably affected.

CHAPTER V

EXAMPLE OF APPLICATION TO A SPECIFIC ROCKET

To see the magnitude of the effects to be expected for the AVT nozzle, a sample calculation is presented.

Let us assume a contoured nozzle having axial outflow and the following properties:

$$T_c = 4000^\circ\text{F}$$

$$P_{c_o} = 500 \text{ psia}$$

$$A_{t_o} = 4 \text{ in}^2$$

$$A_e = 60 \text{ in}^2$$

$$k \text{ of exhaust gas} = 1.285$$

$$\text{molecular wt. of gas} = 28$$

$$C_D = .98$$

These result in the following:

$$A_e/A_{t_o} = 15$$

$$p_e/p_c = 0.0057$$

$$R = 55 \text{ ft lb}_f/\text{lb}_m^\circ\text{R}$$

$$M_{e_o} = 16.0 \text{ lb}_m/\text{sec.}$$

$$V_e = 6600 \text{ fps}$$

$$F_o = 3453 - 60 \text{ Pa}$$

$$P_c = 500 \left[\frac{A_t}{A_{t_o}} \right]^{\frac{1}{n-1}}$$

$$F = 3280 \left[\frac{A_t}{A_{t0}} \right]^{\frac{n}{n-1}} + 171 \left[\frac{A_t}{A_{t0}} \right]^{\frac{1}{n-1}} - 60 \text{ p}_a .$$

Figures 13 and 14 show the calculated thrust ratios, at sea level pressure and in a vacuum, respectively. Figure 15 shows the corresponding chamber pressure ratios. These are all presented with the pressure exponent, n , as a parameter. Values of n over 0.85 are seldom used because of near instability. However, with proper response time of the secondary system, propellants with n nearer unity should be safe to use.

According to the cold air test indications, the ordinate $\frac{A_{t0}-A_t}{A_{t0}}$, can be replaced by about M_2/M_0 with the scale values reduced to about half.

This example shows that the amplification in thrust is accompanied by an almost equal amplification of chamber pressure, which restricts the variation due to strength limitations. If the rocket case is designed for the overpressure condition at ignition, this will provide a means of increasing the thrust without added case strength.

CHAPTER VI

CONCLUSIONS AND RECOMMENDATIONS

A secondary injection of gases at the nozzle throat provides a means of producing changes in effective throat area, thereby permitting great variations in thrust when applied to solid propellant rockets. The mechanism is simple, requiring only a regulated pressure valve and a small amount of piping. The response time should be short, and experience with side injection vector control would be applicable in development of controls mechanism.

The combustion chamber pressure is adequate to provide secondary gas giving good area variation. However, such use would aggravate the nozzle throat heating problems. The use of a cold, bottled gas or liquid for the secondary flow would provide nozzle cooling. The throat cooling benefit may be considerable, since an actual displacement of the hot gases from the walls is realized.

Cold air tests indicate that per cent throat area change of about twice the per cent injected-to-primary flow is easily obtained. With nozzles designed specifically for secondary throat injection, AVT nozzles with a magnification of three or more should be possible.

Future research using the existing thrust stand and apparatus in the laboratory should result in many interesting and varied projects with varied nozzle designs and applications. An analysis of the heat transfer characteristics and erosion problems possibly encountered in

the AVT nozzles used in this analysis would serve to be of extreme value under actual operating conditions.

Specific Recommendations

1. The use of hot gases for an analysis of this nature would be extremely worthwhile and should produce valuable results.
2. The determination of the response times of this system should be attempted.
3. Optimization of the injection location and angle should be performed.
4. Better knowledge of the details of the flow phenomenon of transverse injection in a throat region are needed.

Since some difficulties were experienced in the laboratory with air flow leakages utilizing the existing plastic lines, it is recommended that wherever possible, these plastic lines be replaced by copper tubing. This should provide a permanent instrumentation set-up for future research. In addition, this would result in increased accuracy and dependability at high operating pressures.

SELECTED BIBLIOGRAPHY

1. Summerfield, M., "Control of Solid Propellant Burning Rate by Acoustic Energy," A.R.S. Journal, October 1959.
2. Berman, K., and F. W. Crimp, Jr., "Performance of Plug-Type Rocket Exhaust Nozzles," A.R.S. Journal, January 1961.
3. Gates, J. S. and S. L. Pinto, "Thrust Magnitude Control for Solid Propellant Rocket Motors by Mechanical Means," S.A.E. Paper T-59.
4. Rao, G. V. R., "The E-D Nozzle," Astronautics, September 1960.
5. Rodriguez, C. J., "An Experimental Investigation of Jet-Induced Thrust Vector Control Methods," Paper presented at the 17th Annual JANAF-ARPA-NASA Solid Propellant Meeting, Denver, Colorado, May 1961.
6. Hunsaker, J. C. and B. G. Rightmire, Engineering Applications of Fluid Mechanics, McGraw-Hill Book Company, Inc., New York, First Edition, 1947.

APPENDIX

FIGURES

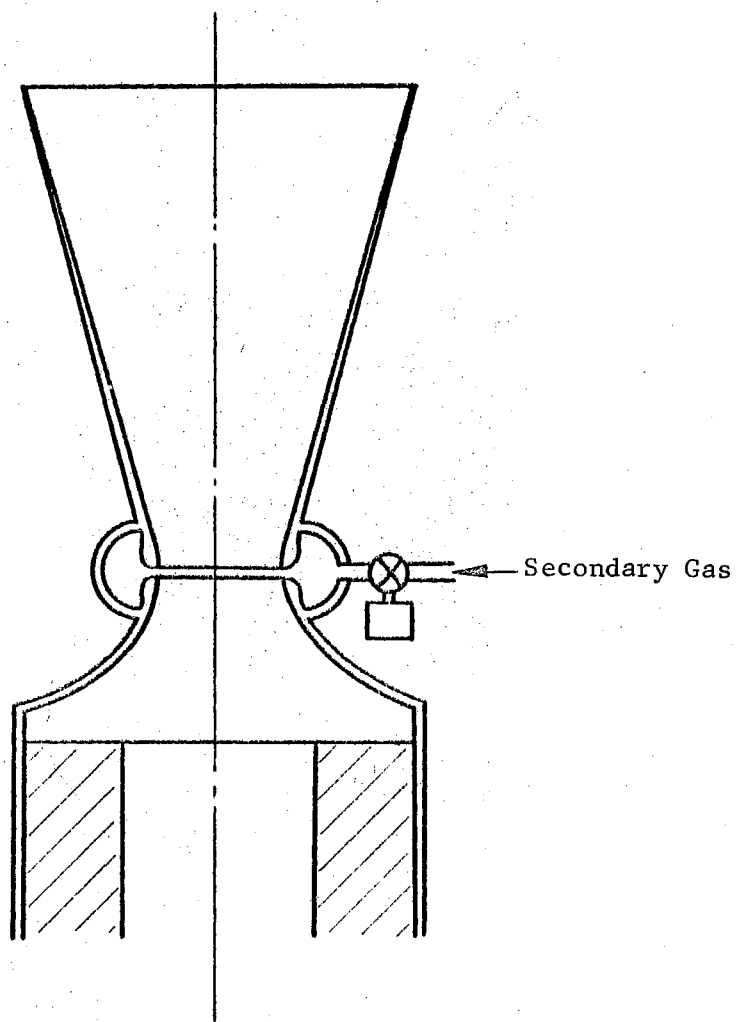


Figure 1. The AVT Nozzle on
a Solid Propellant Rocket.

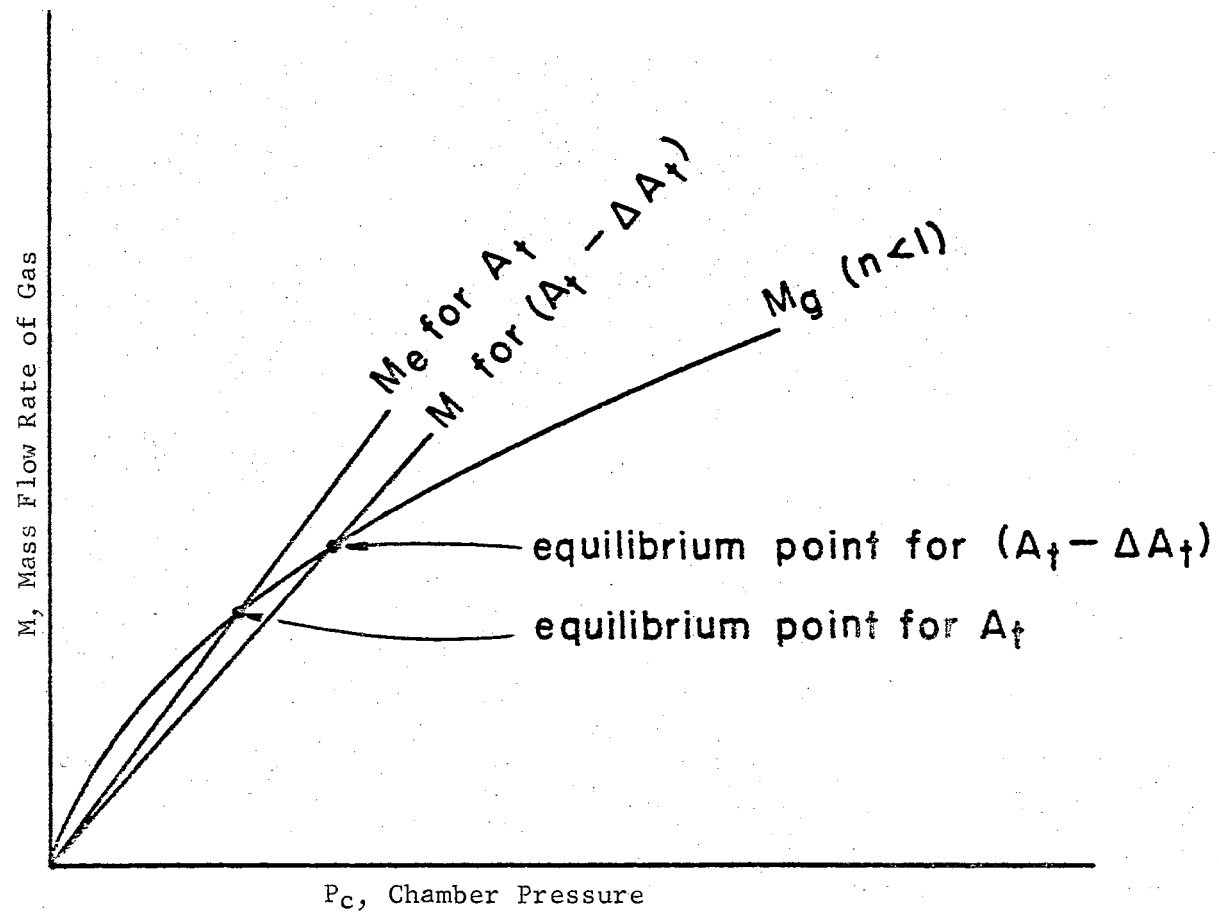


Figure 2. Equilibrium Pressure Conditions for a Solid Propellant Rocket.

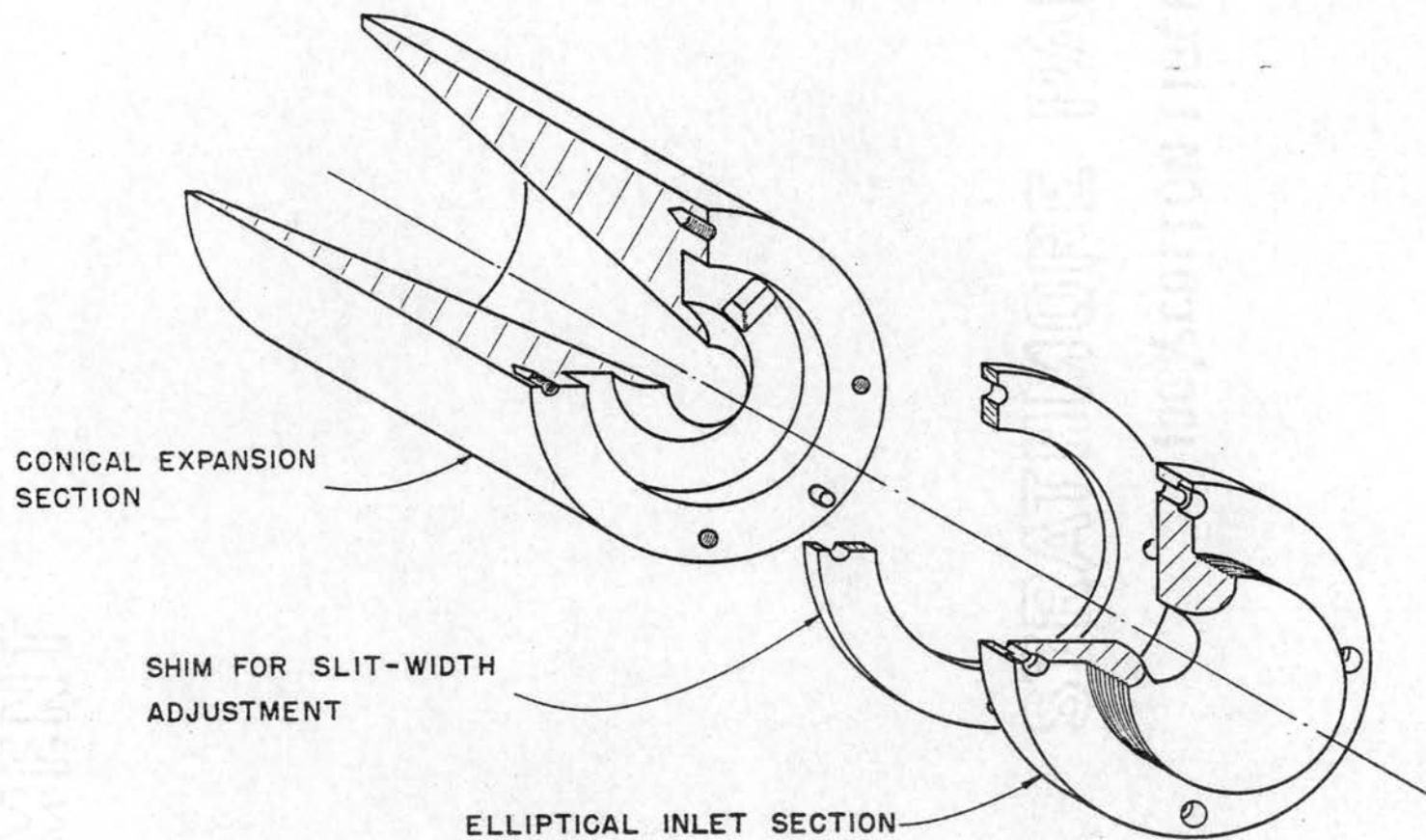


Figure 3. The AVT Nozzle for Air Flow Tests.

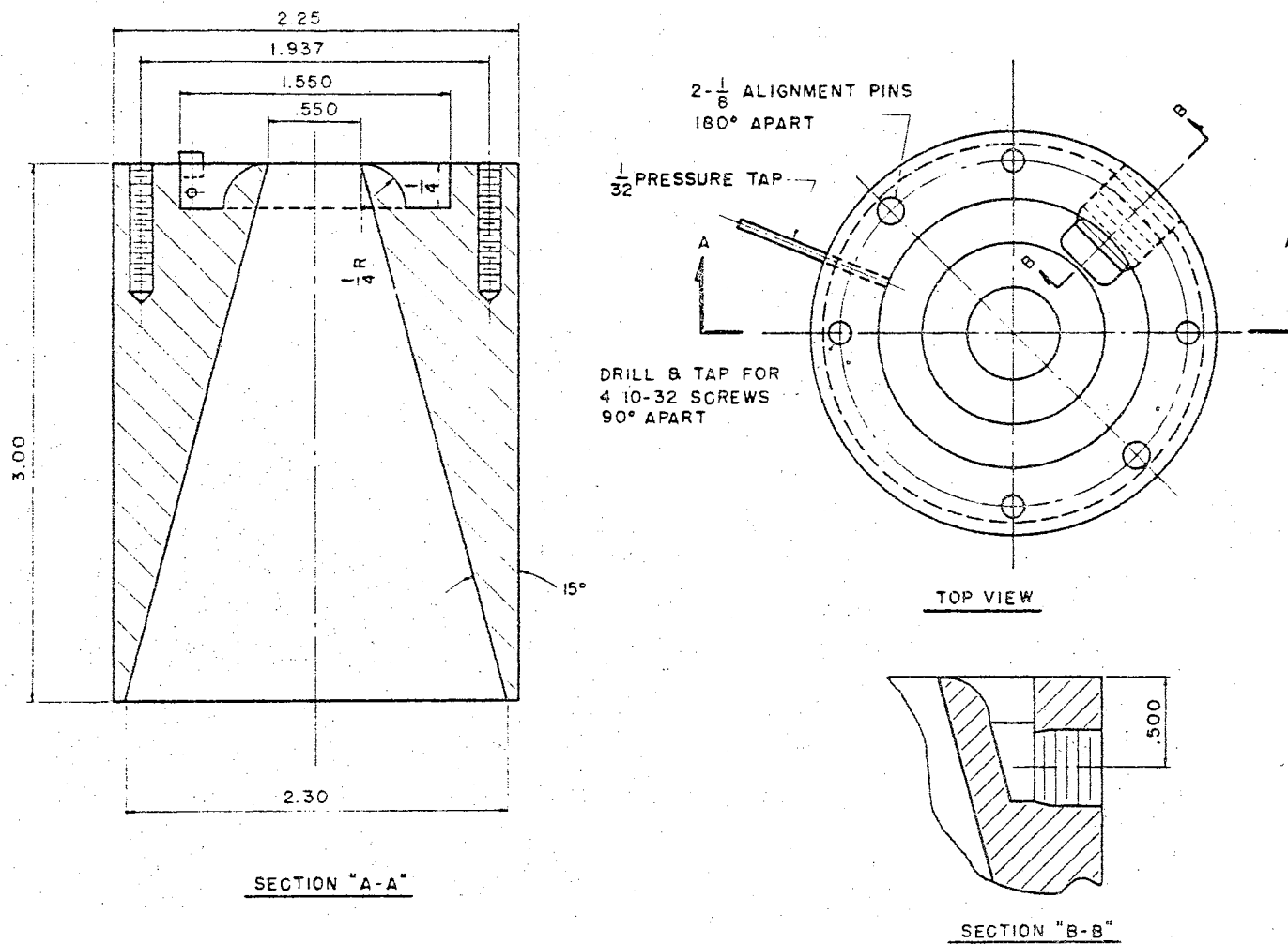


Figure 4. Detailed View of Conical Expansion Section of AVT Nozzle.

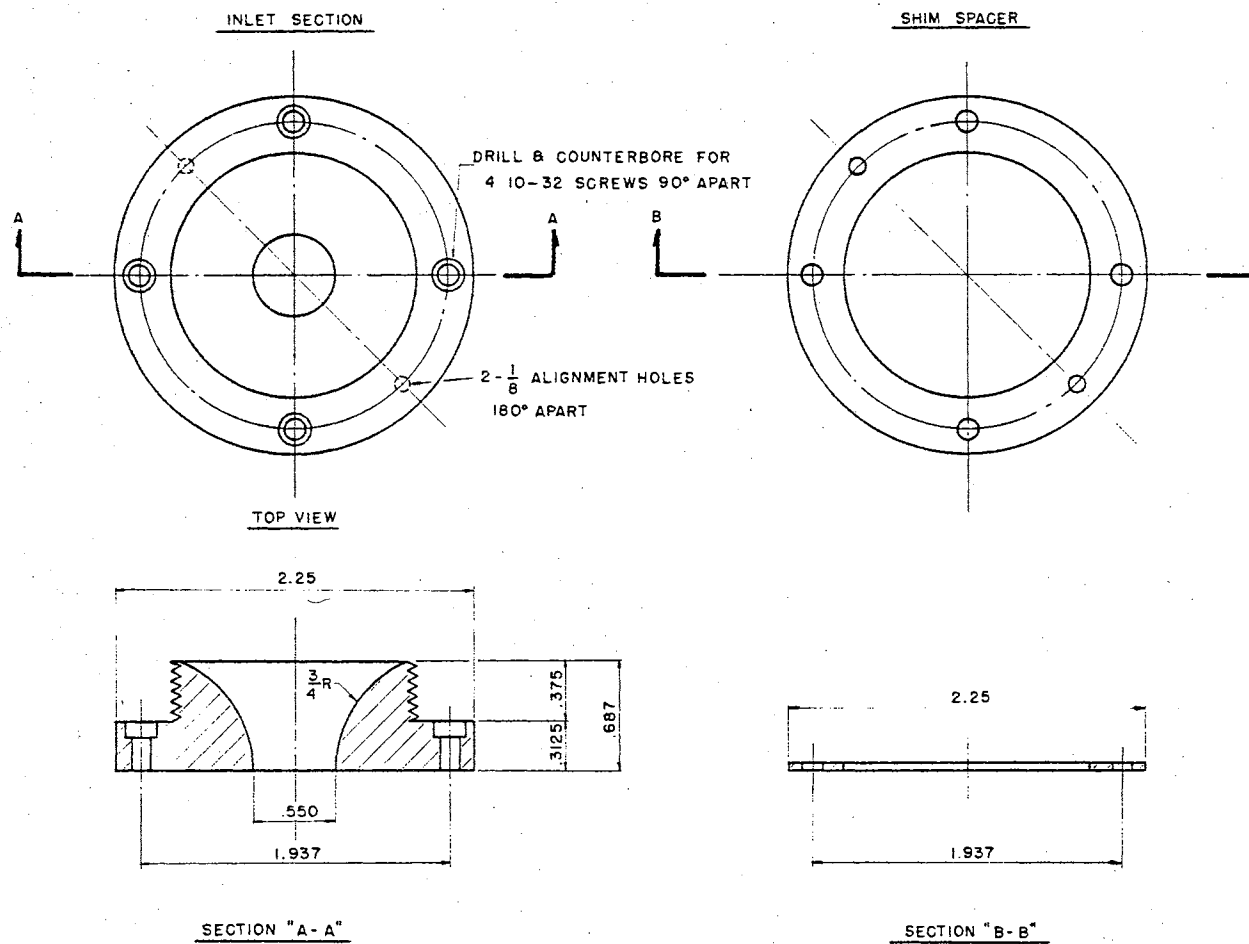


Figure 5. Detailed View of Inlet Section of AVT Nozzle.

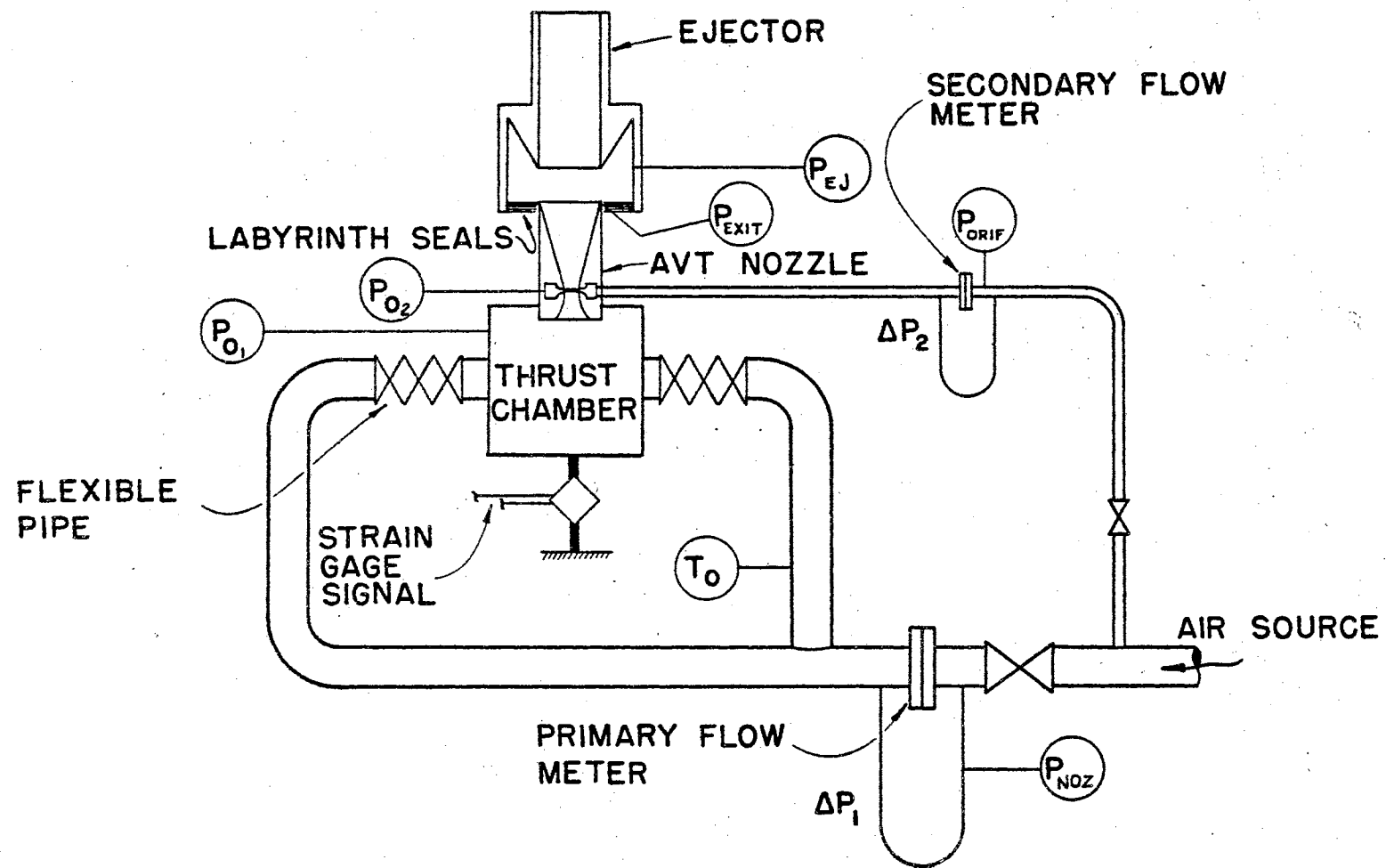


Figure 6. Schematic of Test Set-Up

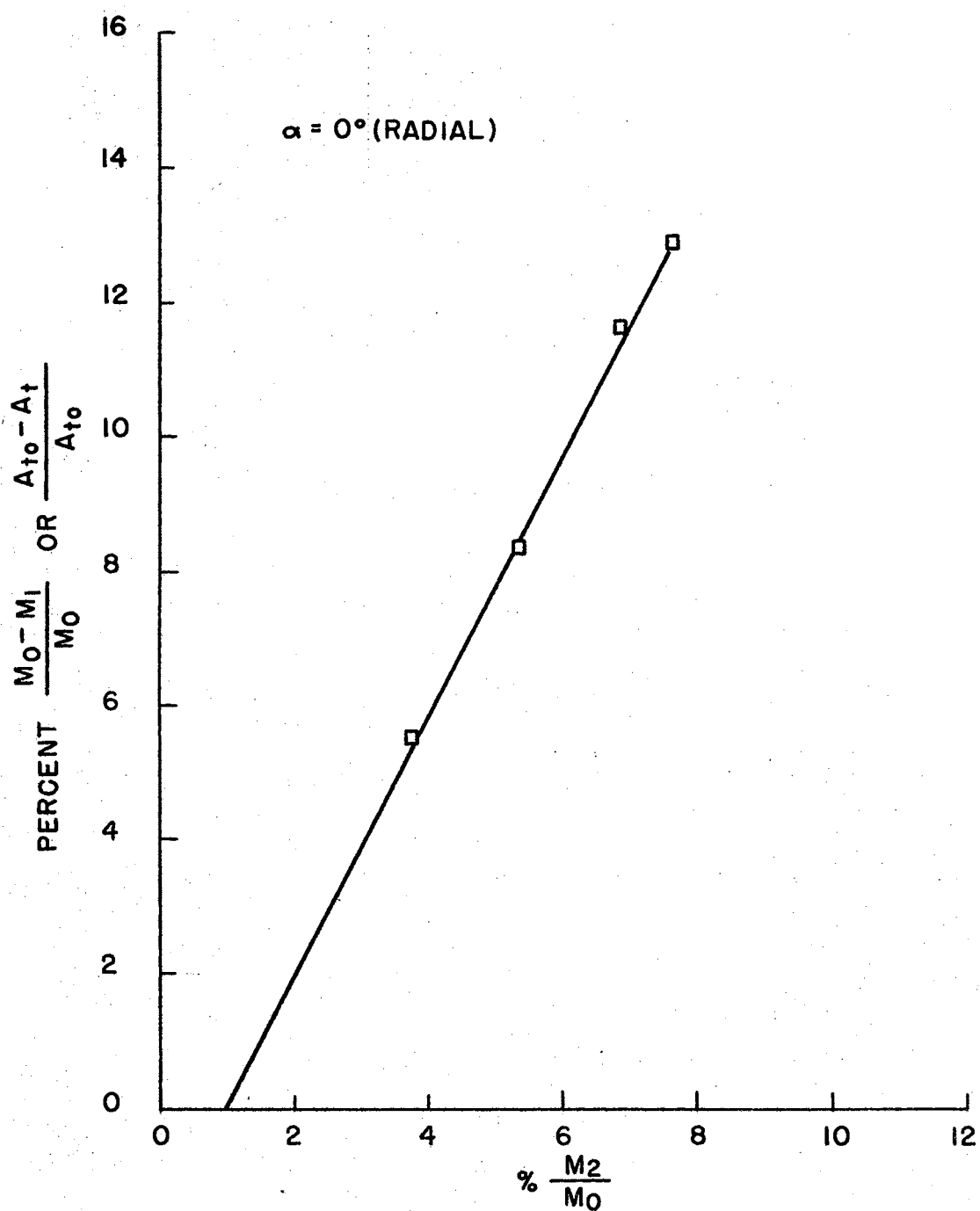


Figure 8. Primary Flow Change for Secondary Flow Rates
(Air Flow Tests, $\alpha = 0$ Degrees).

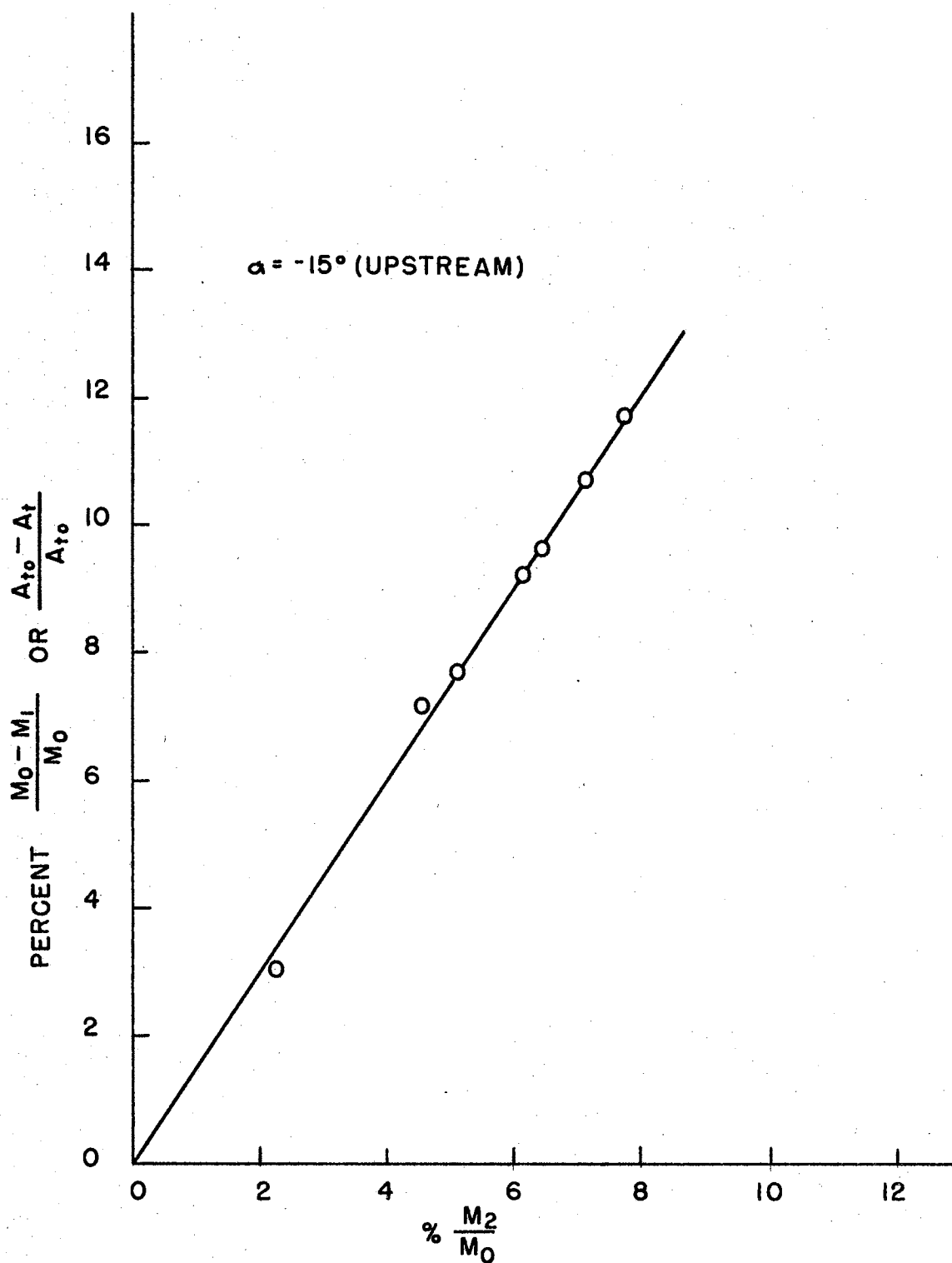


Figure 9. Primary Flow Change for Secondary Flow Rates.
(Air Flow Tests, $\alpha = -15$ Degrees).

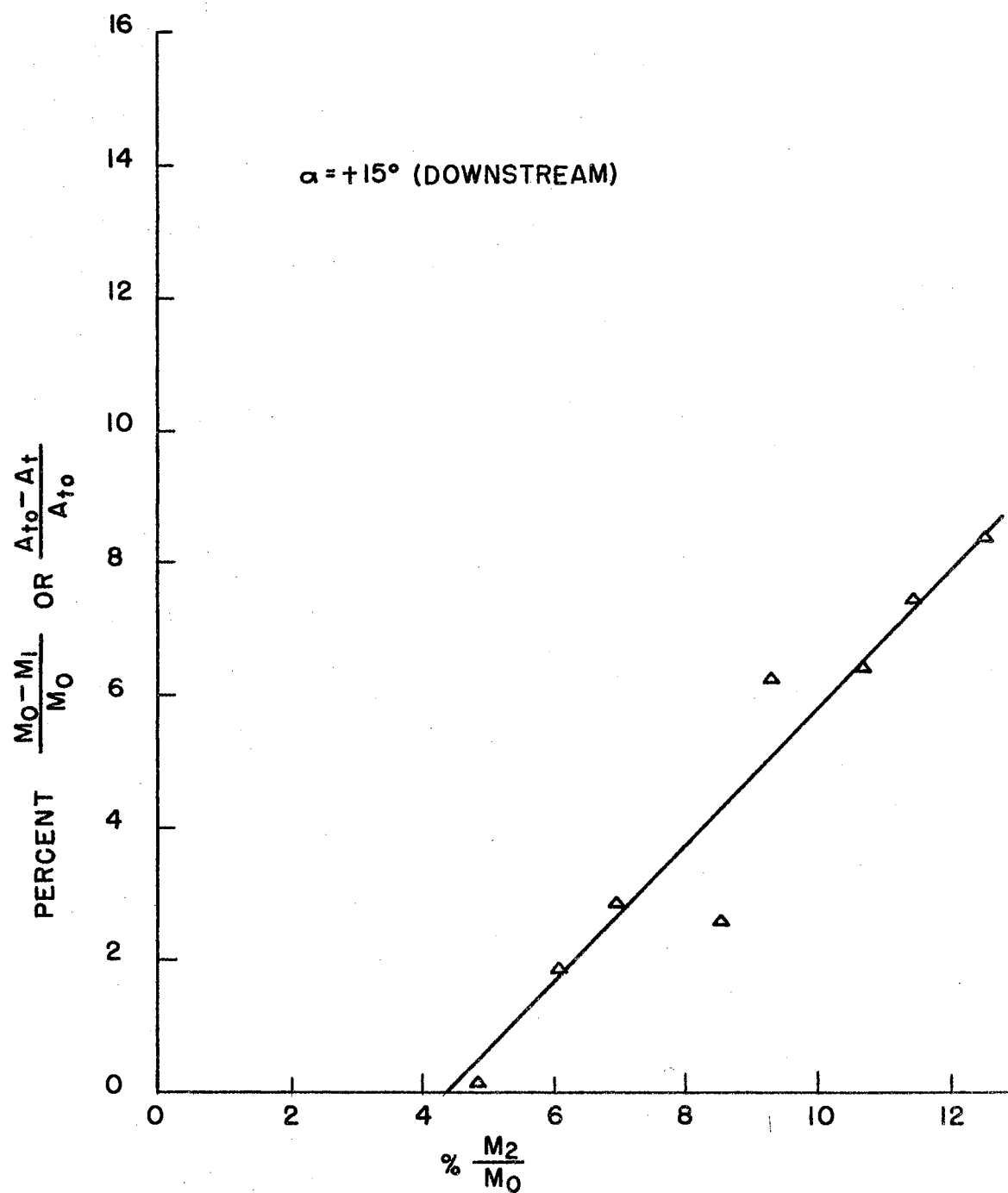


Figure 10. Primary Flow Change for Secondary Flow Rates
(Air Flow Tests, $\alpha = +15$ Degrees).

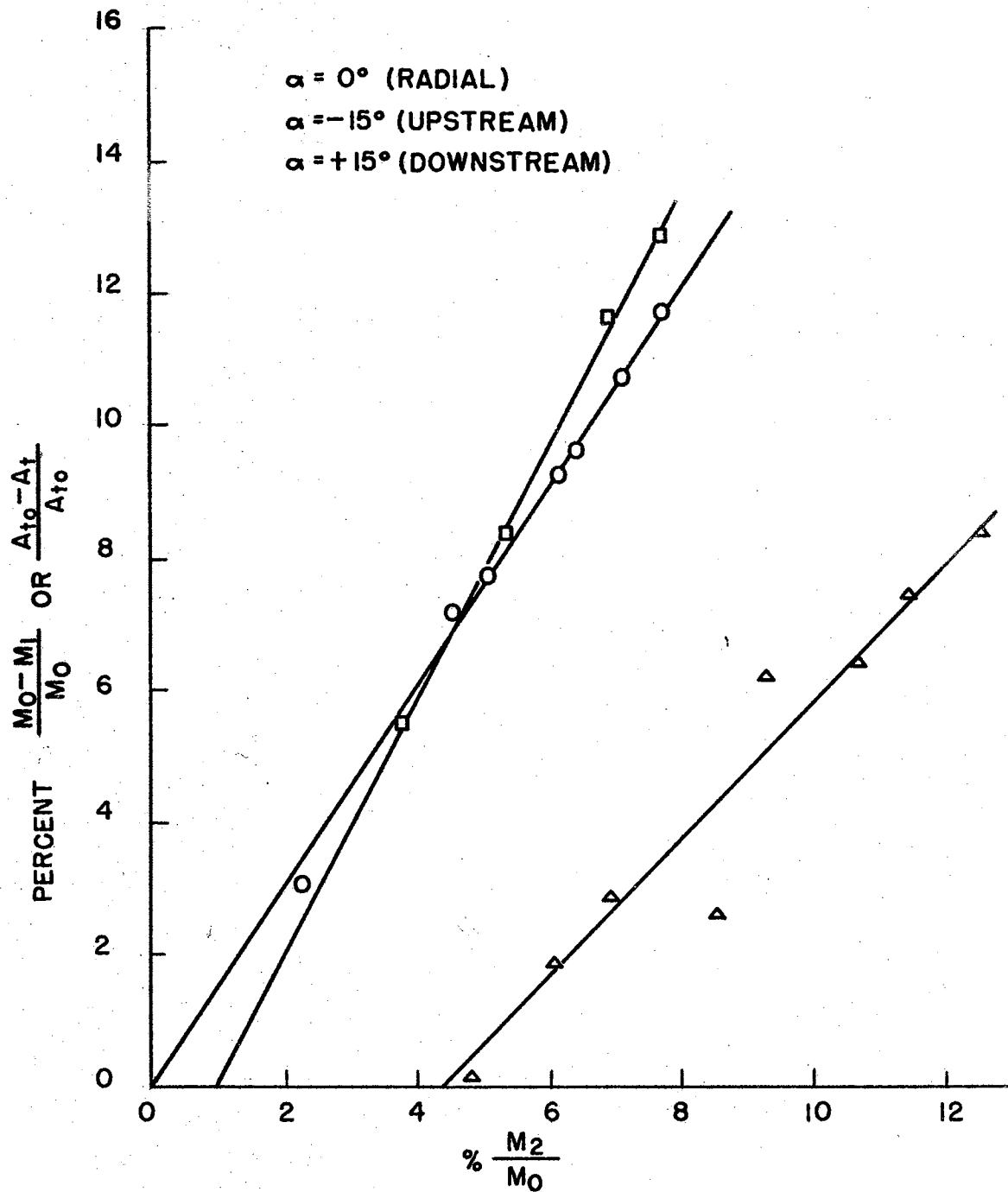


Figure 11. Comparison of Primary Flow Changes for Secondary Flow Rates (Air Flow Tests, $\alpha = 0, -15, +15$ Degrees).

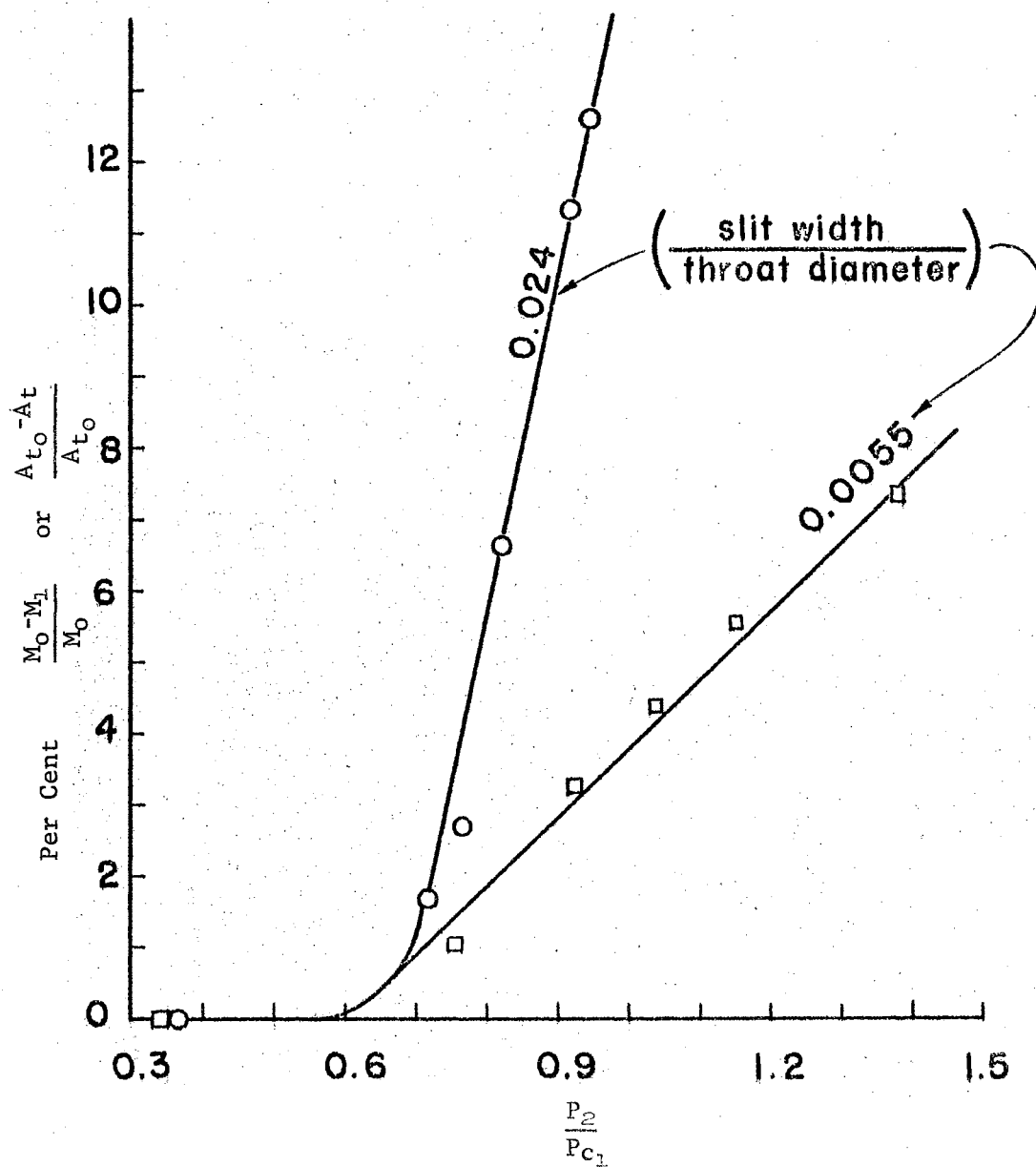


Figure 12. Effect of Secondary Supply Pressure on Primary Flow Change. (Air Flow Tests)

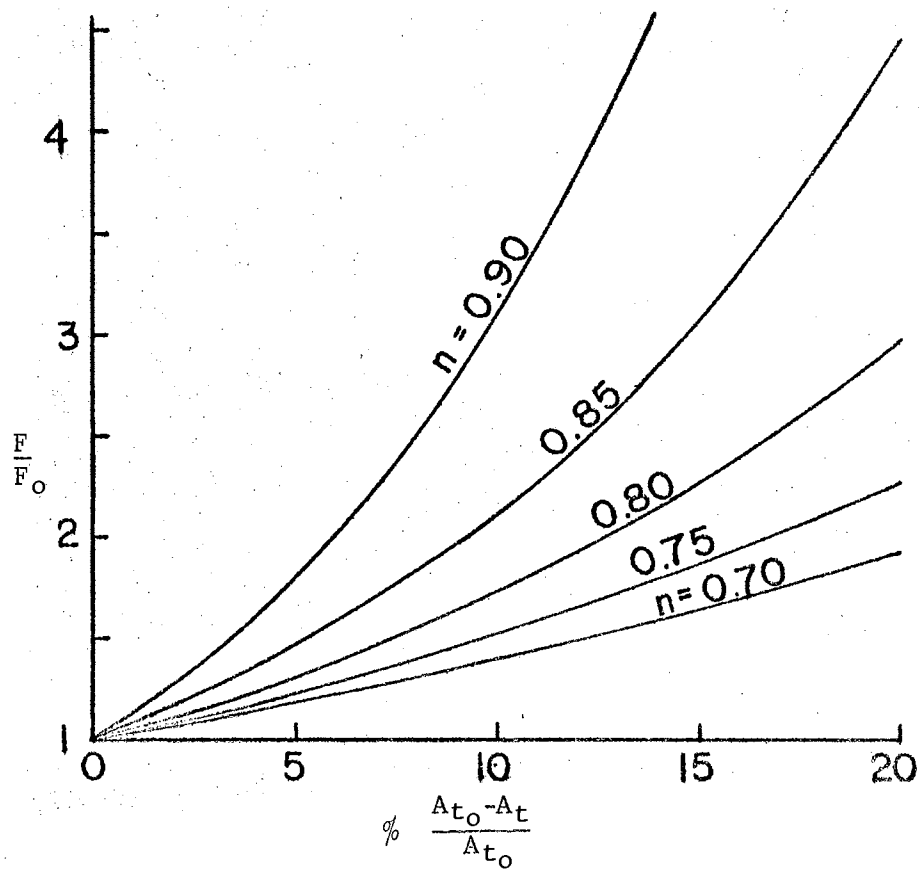


Figure 13. Calculated Thrust Ratio for the Example Rocket at Sea Level.

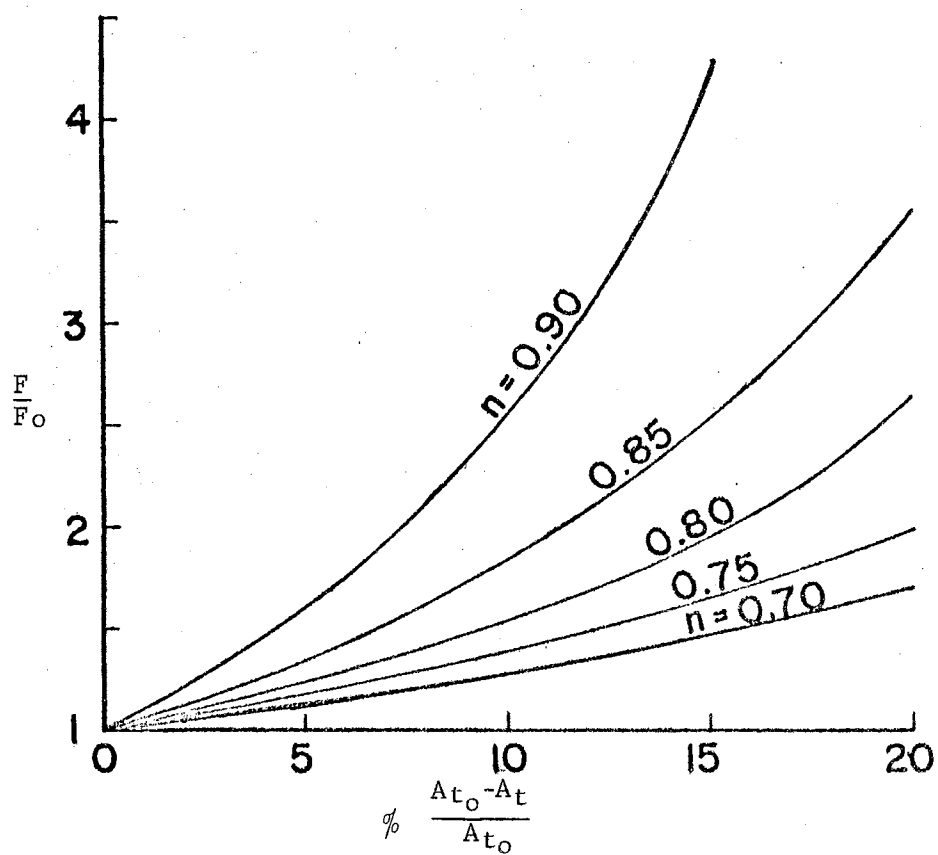


Figure 14. Calculated Thrust Ratio for the Example Rocket in a Vacuum.

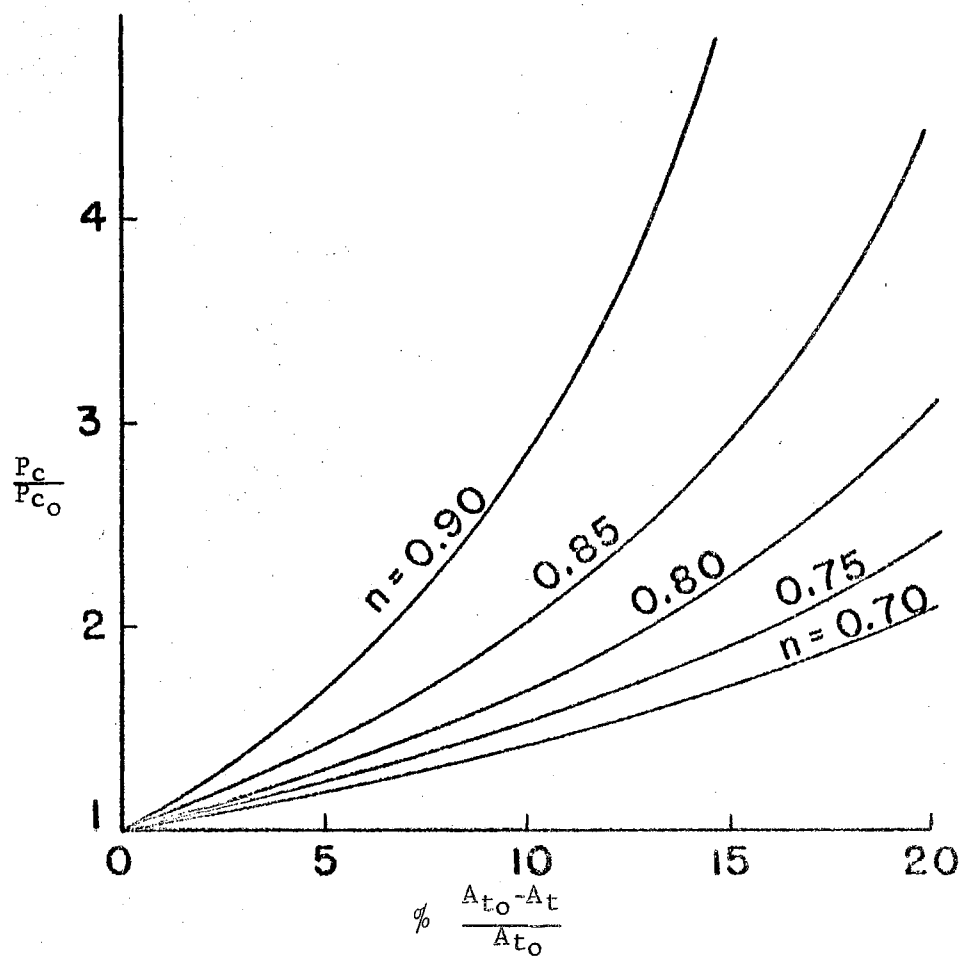


Figure 15. Calculated Chamber Pressure Ratio for the Example Rocket.

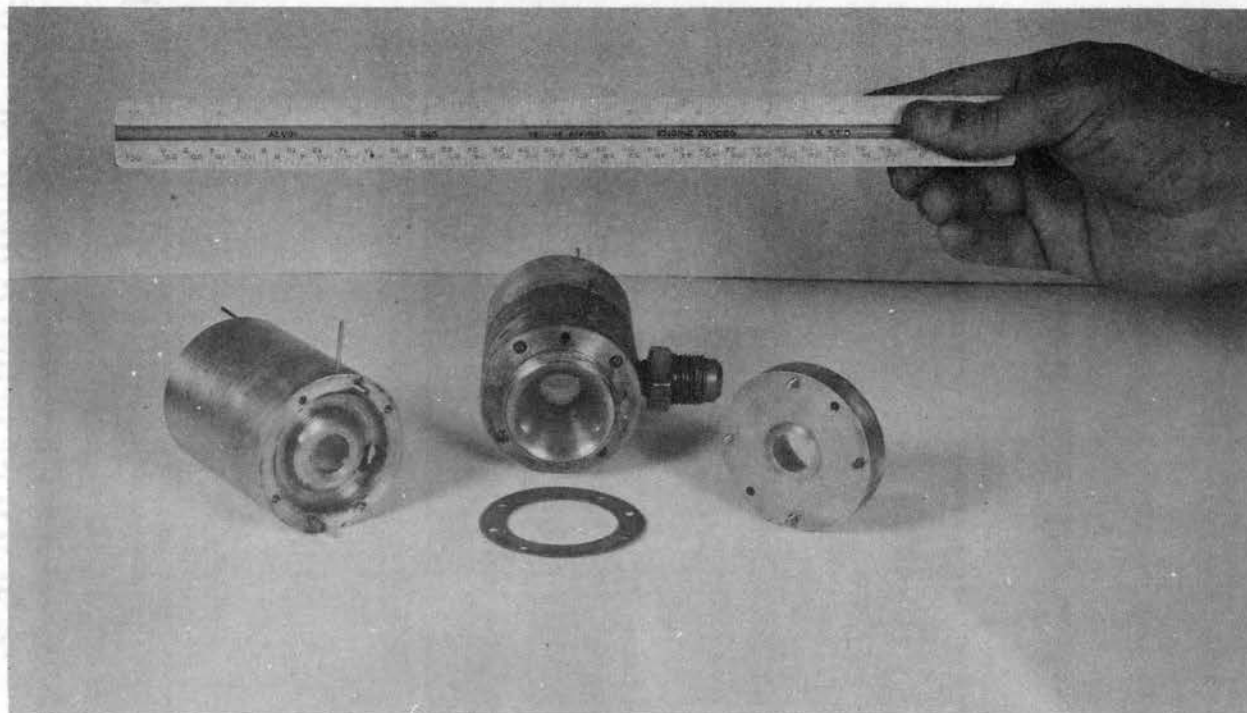


Figure 16. AVT Nozzles Used in Tests.

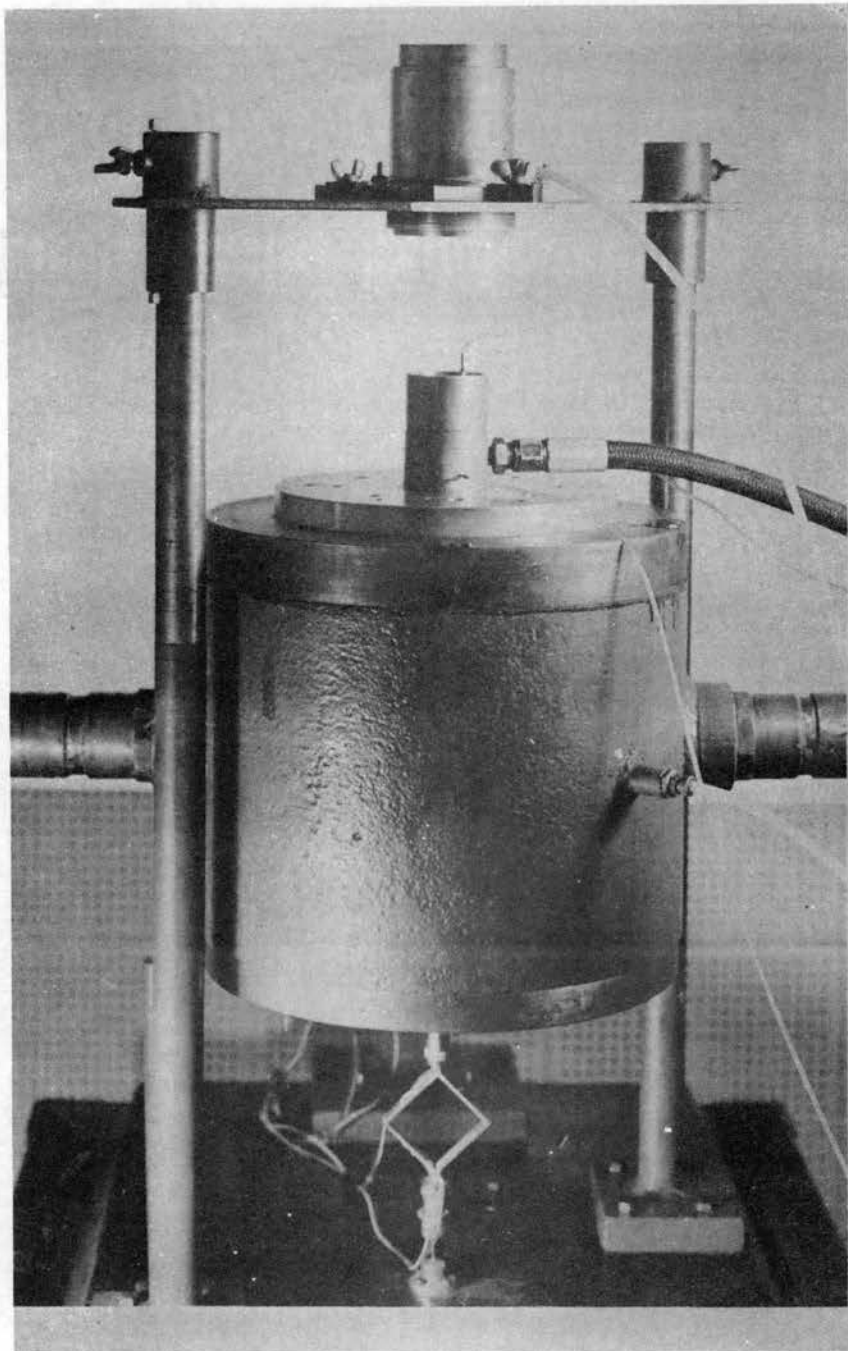


Figure 17. Thrust Stand Apparatus.

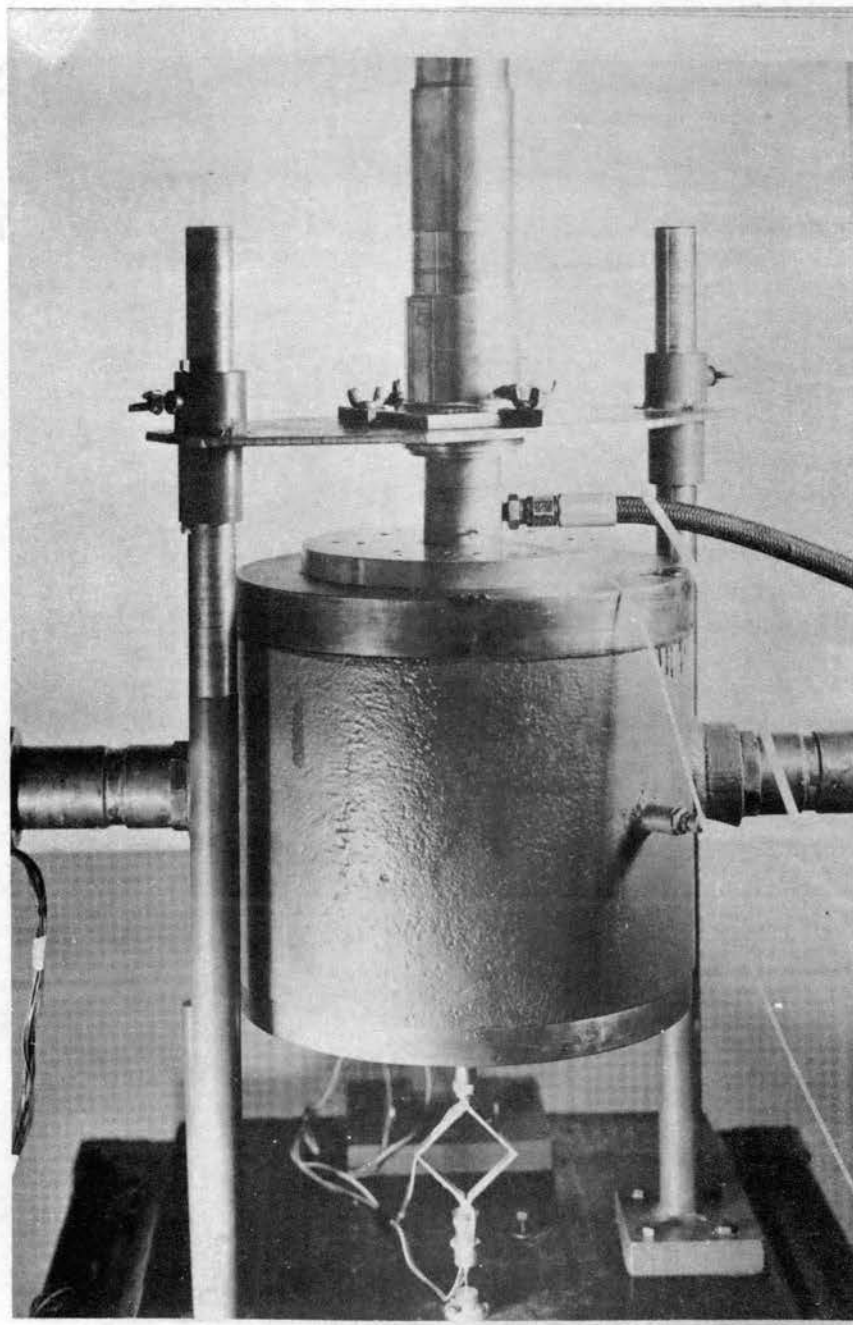


Figure 18. Thrust Stand Apparatus with Ejector
in Position.

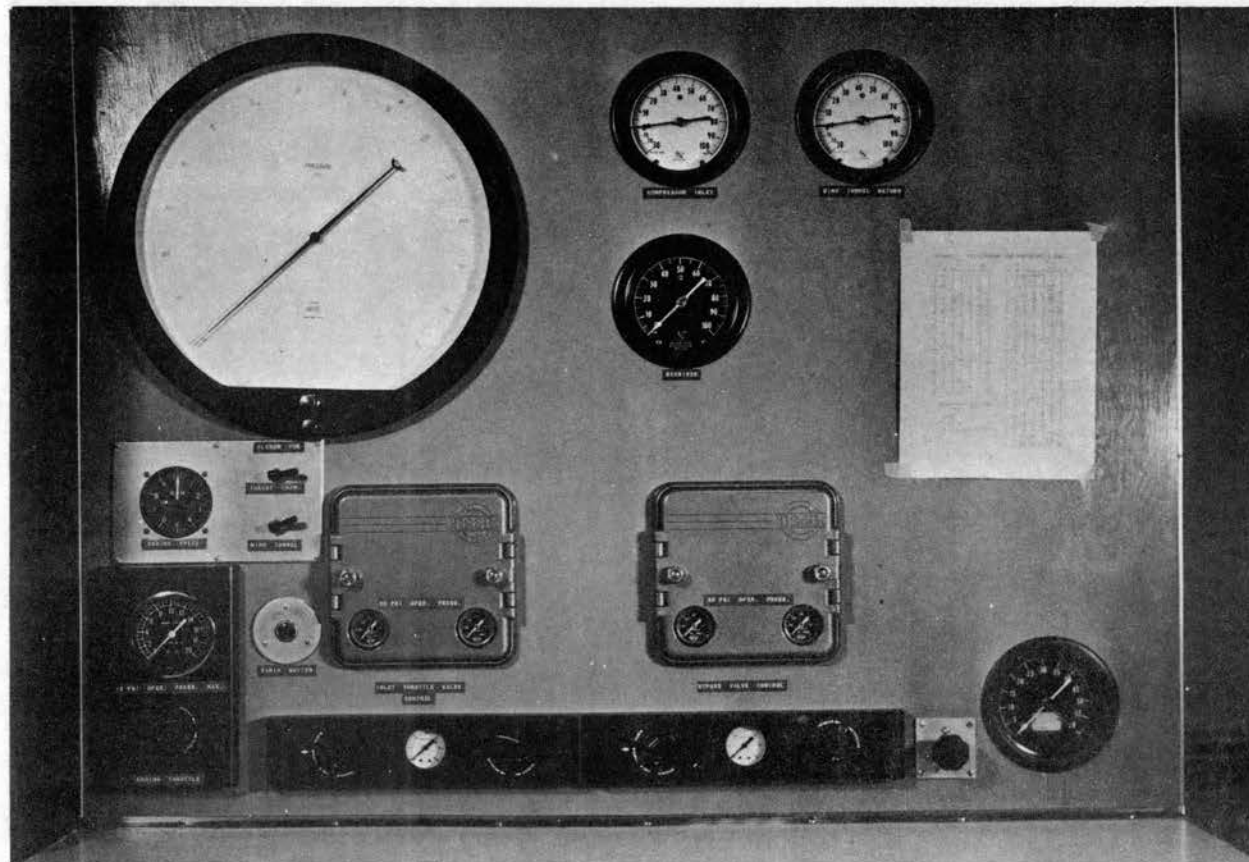


Figure 19. Thrust Stand Control Panel Arrangement
Used in Tests.

VITA

William N. Jackomis

Candidate for the Degree of
Master of Science

Thesis: AN EXPERIMENTAL STUDY OF AERODYNAMICALLY VARIABLE THROAT AREA
(AVT) NOZZLES.

Major Field: Mechanical Engineering

Biographical:

Personal Data: Born in Gary, Indiana, January 17, 1930, the son
of Nicholas and Helen Jackomis.

Education: Graduated from Tolleston High School, Gary, Indiana,
June, 1947. Attended Indiana University - Gary College from
1947 to 1949; Attended U. S. Military Academy, West Point,
New York, from 1949 to 1951; entered the University of Notre
Dame, Notre Dame, Indiana in September, 1951, and received the
Bachelor of Science Degree in Mechanical Engineering in Janu-
ary, 1954. Entered Oklahoma State University in January, 1961,
and completed requirements for Master of Science Degree in
Mechanical Engineering in June, 1962.

Professional Experience: Employed as Petroleum Sales Engineer at
E. I. DuPont de Nemours and Company, Wilmington, Delaware, in
1954. Employed at Inland Steel Company, East Chicago, Indiana,
as a Jr. Field Engineer for two summers, 1952-53. Entered the
U. S. Air Force in June, 1954, and currently serving on active
duty in grade of Regular Captain. Served overseas at Harmon
AFB, Newfoundland, as a Jet Fighter Pilot and Administrative
Officer from 1955 to 1958. Served as Helicopter Flight Test
Pilot and Standardization Instructor Pilot (26th Air Division,
ADC) while stationed at Suffolk County AFB, Long Island, New
York from 1958 to 1961.

Professional Organizations: Institute of Aerospace Sciences.